High-Frequency Combustion Instabilities in Liquid Rocket Engines Driven by Propellants Flow Rate Oscillations

Robin Nez, Thomas Schmitt, Sébastien Ducruix

High-Frequency Combustion Instabilities in Liquid Rocket Engines Driven by Propellants Flow Rate Oscillations

Robin Nez[a,b], **Thomas Schmitt**[a], **Sébastien Ducruix**[a]

[a] *Laboratoire EM2C, CNRS, CentraleSupélec, Université Paris-Saclay, Bâtiment Eiffel, CentraleSupélec, 3 rue Joliot Curie, 91192 Gif-sur-Yvette Cedex, France, Email: robin.nez@centralesupelec.fr*
[b] *CNES DLA, 52 Rue Jacques Hillairet, 75612 Paris Cedex, France*

Keywords: Combustion Instabilities, Transcritical Flames, Large-Eddy Simulation, Reduced-Order Modeling, Flame Transfer Function

Abstract:

Acoustic pressure fluctuations within the combustion chamber or the plenums of a liquid rocket engine (LRE) may induce temporal modulations of the injection velocities of the propellants. The dynamic response of a transcritical coaxial flame to such velocity modulations is investigated here as it is thought to be one of the mechanisms that may promote high-frequency combustion instabilities in LREs. This question is addressed through Large-Eddy Simulations (LES) of a single element LOx/GCH_4 coaxial injector, the present work being focused on the case where the annular GCH_4 flow only is modulated. The simulations reveal that when this annular stream is modulated, vortices are produced and travel along the flame front, inducing local flame stretch rate disturbances. A low-order model for this process is proposed and proves to be in fairly good agreement with the results of our simulations both in terms of gain and phase.

1. Introduction

High-Frequency (HF) combustion instabilities have always constituted an important source of failure for liquid propellant propulsion systems. Today it is still one of the main challenges for the development of a Liquid Rocket Engine (LRE), see among others the review by Oefelein and Yang [1]. These instabilities are due to a resonant coupling that can occur between acoustics, hydrodynamics and combustion, see Culick [2], Yang and Anderson [3]. Under certain conditions, this coupling may constitute a closed-loop dynamical system which may then lead to self-sustained pressure oscillations. It is of prime importance to predict these unstable operating conditions and for that purpose to develop engineering modeling tools to decrease the need for hot-fire tests and reduce engine development costs. Large-Eddy Simulation (LES) constitutes a promising approach (see Hakim *et al.* [4] and Urbano *et al.* [5]), but currently available computational resources make it too expensive to be used as a design tool in the space propulsion industry. Much effort is consequently put into the development of reduced-order modeling tools (Candel *et al.* [6], Pieringer *et al.* [7], Hakim *et al.* [8], Schulze and Sattelmayer [9]). These tools are designed to perform stability analyses or to predict limit cycle oscillations at the expense of a reduced computational demand. However, they require submodels to account for the dynamic response of the flames to the acoustic or hydrodynamic perturbations and then require a significant modeling effort. As many flame response models are required as there are thermoacoustic coupling mechanisms at play in the engine. Pressure oscillations within the combustion chamber and/or the injection manifolds can modulate the pressure drop across an injector element and consequently excite the flame. This has already been observed within lab-scale experiments, see for instance the observations reported by Noiray *et al.* [10]. One possible coupling mechanism could then be associated with the fluctuating injection velocity of one of the propellants. As experimental diagnostics are usually limited by the extreme conditions prevailing in configurations typical of LREs, LES is increasingly used to study flame dynamics and to provide validation data to reduced-order models. The dynamics of a transcritical coaxial flame under transverse acoustic forcing were for example simulated by Hakim *et al.* [11]. The objective of the present work is to propose a model for the heat release rate response of a fuel-modulated transcritical coaxial flame and to carry out simulations for validation. The purpose of such a submodel would be to be implemented in a stability analysis tool as a Flame Transfer Function (FTF) for example. In section 2, the numerical setup and the flow solver are briefly described. In section 3, the dynamics of the flame modulated at several frequencies are qualitatively analyzed. In section 4, a reduced-order model accounting for the production and convection of flame stretch rate disturbances is derived and confronted to the simulations. Conclusions are drawn in section 5.

2. Numerical setup

2.1. Geometry and load point

The setup corresponds to the configuration studied by Hakim *et al.* [11]. The domain consists in an almost cubic chamber, equipped with a single shear coaxial element on one end and a small exhaust pipe on the other. The main dimensions of the chamber are given in Figure 1a.

The dimensions of the shear coaxial injector are quoted in Figure 1b. The injector dimensions can be compared to those found in the G2 experimental setup studied by Singla *et al.* [12] on the Mascotte test rig from ONERA, which was itself designed to reproduce conditions typical of actual engines. It can nonetheless be noted that in the present configuration the dimensions of the chamber are large compared to those of the injector element. This is to avoid any confinement effect on the flow dynamics in order to facilitate the analysis of the phenomena of interest. Another substantial specificity of the present geometric setup compared to the aforementioned experiment or real engine injectors is that the LOx post is not tapered. This is to allow for coarser mesh resolutions in the vicinity of the injector, thus facilitating extensive parametric investigations at lower CPU costs.

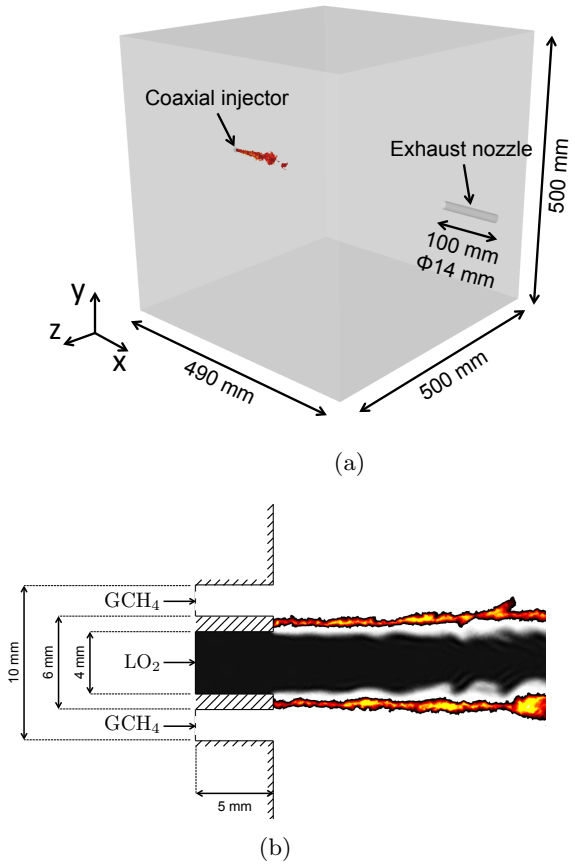

Figure 1: Depiction of the computational domain and dimensions of the injector.

The mean chamber pressure is stabilized to 1.17×10^7 Pa. This is well above the critical pressures of methane as well as oxygen and Hakim *et al.* [11] demonstrated that, depending on the mixture fraction, the burnt mixture can either be supercritical or in a gaseous state (subcritical pressure but supercritical temperature). No two-phase flow regime can then be encountered in this configuration. The details of the injection parameters are given in Table 1. The mixture ratio E and the momentum flux ratio J are defined as follows:

$$\mathrm{E} = \frac{\dot{m}_{\mathrm{O_2}}}{\dot{m}_{\mathrm{CH_4}}}, \tag{1}$$

$$\mathrm{J} = \frac{\rho^0_{\mathrm{CH_4}} (u^0_{\mathrm{CH_4}})^2}{\rho^0_{\mathrm{O_2}} (u^0_{\mathrm{O_2}})^2}. \tag{2}$$

The values of these parameters are quite similar to those of the C-60 configuration studied in the Mascotte test rig and further details can be found in Juniper *et al.* [13].
The chamber is initially filled with pure methane and the temperature set to the equilibrium temperature corresponding to the load point. The annular GCH_4 stream is modulated by prescribing a sinusoidal incoming acoustic perturbation at the stream's inlet boundary. The amplitude of the prescribed acoustic velocity signal is about 10% of the annular bulk velocity *i.e.* 20 m.s^{-1}. Eight separate modulated simulations have been performed, with forcing frequencies of 500 Hz, 1000 Hz, 1300 Hz, 2000 Hz, 2750 Hz, 3500 Hz, 5000 Hz and 8000 Hz. A reference simulation with no modulation has also been performed so that the effects of the modulation can be easily assessed. After a transient period, each simulation is run over 64 ms for statistical convergence.

2.2. Flow solver

The present Large Eddy Simulations are carried out using the flow solver AVBP developed at CERFACS and IFPEN. It is used to integrate the filtered three-dimensional compressible Navier-Stokes equations for reacting multispecies mixtures on unstructured meshes (Schönfeld and Rudgyard [14], Gourdain *et al.* [15]). The discretization employs a Two-Step Taylor-Galerkin scheme (TTGC) which is third-order in space and time (Colin and Rudgyard [16]). Characteristic boundary conditions (Thompson [17], Poinsot and Lele [18]) are employed to allow the acoustic forcing of the computational domain, as well as to control the amount of acoustic energy entering and leaving the domain, see Selle *et al.* [19]. AVBP's real-gas extension (Pons *et al.* [20], Schmitt *et al.* [21, 22]) employed in the present calculations and developed at EM2C and CERFACS takes into account thermodynamic non-idealities through the use of cubic equations of state, the Soave-Redlich-Kwong (SRK) equation being employed here (Soave [23]). The real-gas transport properties are represented by making use of Chung's laws (Chung *et al.* [24]). Numerical schemes and characteristic boundary conditions are adapted to comply with the real-gas thermodynamics. Subgrid-scale momentum fluxes are modeled by the Wall Adapting Large Eddy (WALE) model (Nicoud and Ducros [25]) as it is well-suited for shear flows, its eddy-viscosity vanishing in purely strained regions of the flow. Subgrid-scale energy and species fluxes are approximated by constant turbulent Prandtl and Schmidt numbers $\mathrm{Pr}_t = \mathrm{Sc}_t$

Table 1: Load point describing parameters.

LOx post		GCH_4 post		Global parameters	
$\dot{m}_{O_2}$ [g.s^{-1}]	423	$\dot{m}_{CH_4}$ [g.s^{-1}]	860	p_c [MPa]	11.7
$T^0_{O_2}$ [K]	100	$T^0_{CH_4}$ [K]	300	E [-]	0.492
$\rho^0_{O_2}$ [kg.m^{-3}]	1122	$\rho^0_{CH_4}$ [kg.m^{-3}]	88	J [-]	3.29
$u^0_{O_2}$ [m.s^{-1}]	30.0	$u^0_{CH_4}$ [m.s^{-1}]	194.4		
Re_{O_2} [-]	7.80×10^5	Re_{CH_4} [-]	5.48×10^6		

= 0.75. Chemical conversion is represented with the infinitely fast chemistry model IFCM described in Schmitt *et al.* [22]. It was shown by Pons *et al.* [26] that, for stretched counter-flow high pressure methane-oxygen flames, chemical times defined as the inverse of the extinction strain rates are always several orders of magnitude below the characteristic mixing and acoustic times related to the present numerical configuration. Equilibrium mass fractions are then tabulated in terms of the mixture fraction and its variance which are both transported, and the following species are retained in order to properly estimate the equilibrium burnt gases temperature at any mixture fraction: CH_4, O_2, CO_2, H_2O, CO and H_2. The species source terms are then computed according to the procedure detailed by Schmitt *et al.* [22]. Injector walls are treated as Neumann boundary conditions through the enforcement of wall stresses deduced from a mixed law of the wall (typical logarithmic law or linear law depending on the local mesh resolution). Synthetic anisotropic turbulence is injected at the domain inlets by enforcing mean and RMS profiles for each velocity component as well as for deviatoric Reynolds stresses. These profiles result from the LES of a periodic pipe flow setup with similar Reynolds number and grid resolution. This synthetic turbulence field is defined by construction of a set of solenoidal modes employing the method proposed by Kraichnan and Celik [27], so that no acoustic noise is produced. This set of modes ends up constituting a Passot-Pouquet spectrum [28]. The tetrahedral mesh employed counts 2.5×10^6 vertices (14.5×10^6 elements). It is refined within the highly stratified region around the dense oxygen jet, with the finer resolution corresponding to 7 elements per injector lip thickness and 25 elements per LOx post diameter and gradually coarsened further downstream.

3. Flow dynamics

For the sake of clarity and conciseness, the comparison of only some of the simulations is presented here. The set of points selected allows an adequate analysis of the effects of the modulation frequency on the overall flame dynamics. However all simulated operating points will serve the comparison with the flame response model derived later on.

3.1. Instantaneous and phased-locked flow visualizations

The main characteristics of the reactive coaxial jet flows resulting from both modulated and non-modulated computations are illustrated by instantaneous snapshots in Figure 2. The red iso-contour of oxygen mass fraction is here employed as a tracker of the flame front. The inner dense jet gets corrugated, the strong density gradients then rapidly decaying downstream due to the enhanced mixing. The inner jet also tends to shed dense oxygen pockets in an intermittent fashion. The light annular jet opening angle is quite low for this kind of setup, and the oxygen mass fraction iso-line demonstrates that the reactive region remains close to the inner oxygen core. Examination of the modulated cases snapshots evidences the dependency of the flow dynamics on the forcing frequency. While lower frequency cases do not significantly depart from the non-modulated case dynamics, modulation at higher frequency proves to induce shorter hydrodynamic disturbances having a much clearer effect on the overall dynamics. At lower frequencies, 'high' and 'low' velocity regions are hardly distinguishable as hydrodynamic wavelengths are of the order of the flame length, the flame being then hydrodynamically compact. At higher frequencies the flame gets significantly non-compact. These shorter vortical structures tend to cause the early destabilization of both streams. Due to the more intense viscous dissipation resulting from their shorter scales, these energetic coherent structures rapidly decay, and even disappear within fully developed turbulence scales even before flowing past the flame tip. All these observations appear much more clearly when looking at phase-locked solutions: each set of flow fields corresponding to a same phase angle with respect to the inflow modulation is averaged. This results in canceling all flow modes except those whose frequency is equal to that of the inflow modulation. In such a way, the chaotic turbulent fluctuations are hidden, and the modulation-induced coherent flow patterns are visible. Phase-locked solutions corresponding to two phase angles are given for three different operating points on Figure 3.

3.2. Spectral analyses

Examining the Power Spectral Density (PSD) of velocity signals recorded in the annular destabilizing jet (2 mm

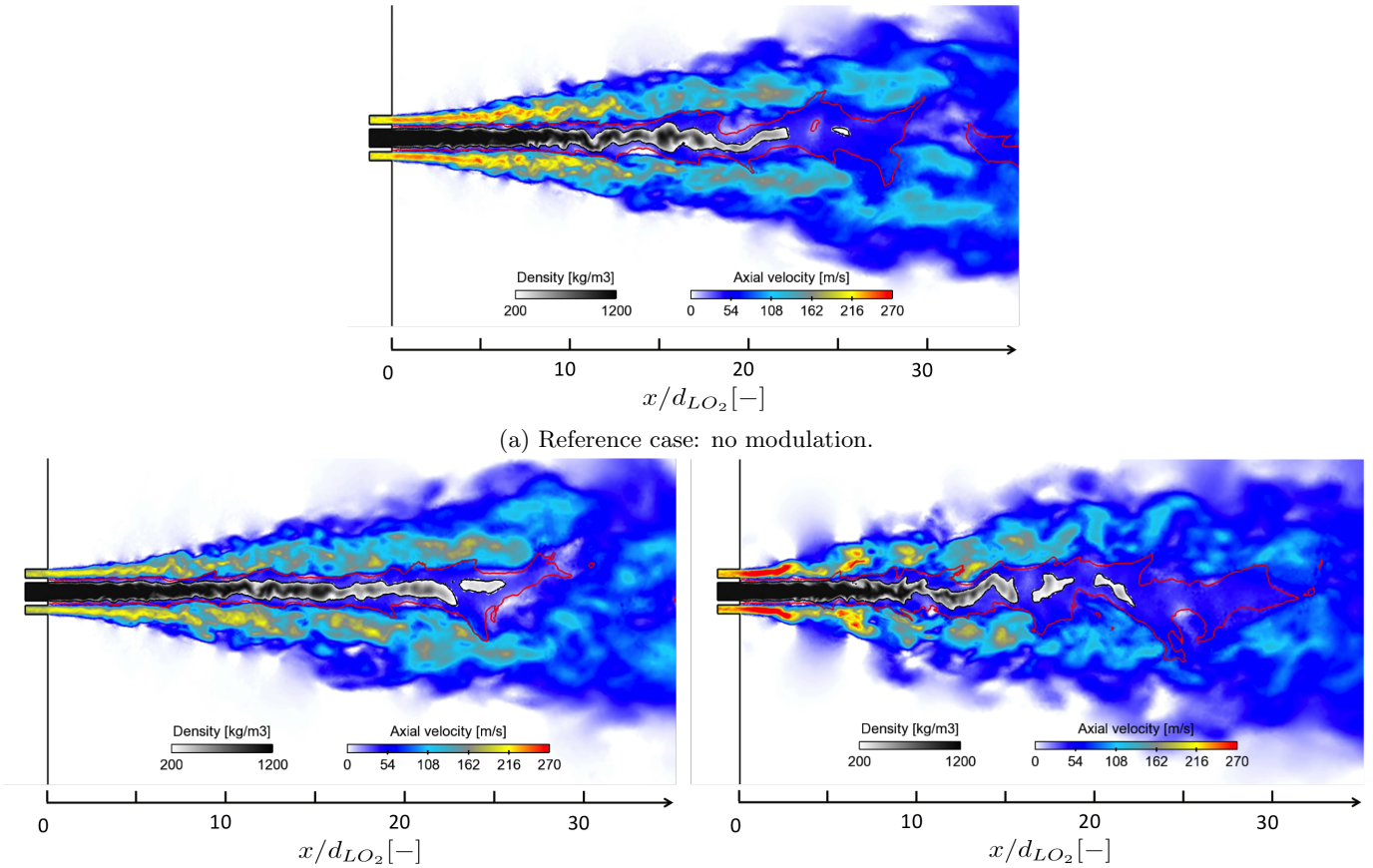

(a) Reference case: no modulation.

(b) 1000 Hz modulation.

(c) 8000 Hz modulation.

Figure 2: Superimposed instantaneous cuts of axial velocity (white to red) and of density within the dense oxygen jet (gray scale). Red: iso-contour of oxygen mass fraction $Y_{O_2} = 0.5$.

from the injector) gives additional insight into the jet dynamics, see Figure 4. The signature of the modulation is always visible, the modulation frequencies being revealed by vertical dashed lines. It is especially interesting to point out the gradual increase of the response amplitude with the forcing frequency for the radial velocity component, whereas it remains fairly constant for every modulation frequency for the axial component. This illustrates again the production of shorter coherent structures at higher forcing frequencies. Additionally, high-frequency harmonics are revealed for 3500 Hz, 5000 Hz and 8000 Hz operating points. A PSD of the computational domain-integrated heat release rate is given in Figure 4 as well. It shows a strong response of the flame to the modulation, regardless of the forcing frequency. The strong signal-to-noise ratio obtained for each case is favorable to the determination of accurate transfer function estimates from the LES signals.

3.3. Effect of the modulation on the mean flow

Before tackling the question of the heat release rate response, it is worth examining its mean spatial distribution for each frequency of modulation. For that sake, the time-averaged heat release rate is integrated over thin slices extending over the full domain in the transverse directions. The resulting data is plotted in Figure 5. While a slight upstream displacement of mean heat release rate is observed when going towards higher frequencies, all profiles are still fairly similar. The modulation does not strongly impact the mean flow, which is in favor of the construction of a linear reduced-order model.

4. Reduced-order modeling

Considering the previous observations from the LES results, the present problem can be schematically represented as in Figure 6. A coaxial injector feeds dense oxidizer and light, gaseous-like fuel and establishes a flame that is stabilized in the close vicinity of the lips of the central injection tube. The annular fuel stream is modulated around its mean value. This modulation produces velocity disturbances within the annular jet, which then propagate along the reactive region. These velocity perturbations translate into flame stretch rate disturbances, which in turn can induce fluctuating heat release rates. In the absence of curvature, the flame stretch rate is defined as the velocity field divergence in the plane tangential to the flame sheet (see Poinsot and Veynante [29]):

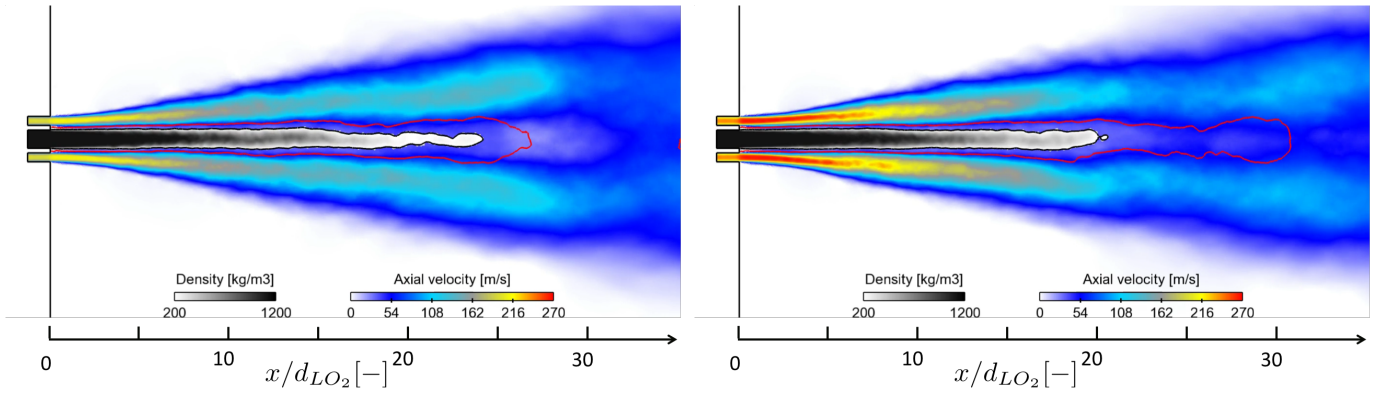

(a) $f = 1000$ Hz, $\phi = 0$.

(b) $f = 1000$ Hz, $\phi = \pi/2$.

(c) $f = 8000$ Hz, $\phi = 0$.

(d) $f = 8000$ Hz, $\phi = \pi/2$.

Figure 3: Superimposed phase-locked cuts of axial velocity (white to red) and of density within the dense oxygen jet (gray scale). Red: iso-contour of oxygen mass fraction $Y_{O_2} = 0.5$.

$$\epsilon = \nabla_t \cdot \mathbf{u}_t, \tag{3}$$

where the subscript t refers to the tangential component of ∇ operator and $\mathbf{u}_t$ is the tangential projection of the velocity field with respect to the flame front. This local tangential plane can be defined as the plane which is locally orthogonal to the gradient of any scalar transported by the flow, for instance mixture fraction, a species mass fraction, or temperature.

4.1. Velocity disturbances propagation

It is first reasonable to assume at this stage that the problem is essentially one-dimensional. This is admittedly not quite right but constitutes a good approximation because the flame expansion is relatively slow. This is justified by recalling that cryogenic flames typically encountered in liquid rocket engines are characterized by large outer to inner momentum flux ratios, typically of the order of 10 or higher. This feature and the significant stratification between the dense inner cryogenic jet and the light annular stream lead to the production of flames with fairly small opening angles. The shed velocity disturbances are associated with a vorticity mode. They are then characterized by a phase velocity of convective nature. As a first approximation, we assume that this phase velocity is equal to the local time-averaged annular jet core velocity $u_0(x)$. This corresponds to expanding this velocity field to first order: $u(x,t) = u_0(x) + u'(x,t)$ and assuming small disturbances around the mean. Now, the traveling velocity perturbation signal may be assumed to be harmonic and may be written in the following form:

$$u(x,t) = u_0(x)(1 + a\sin(\omega t - \kappa(x)x)), \tag{4}$$

where a designates the relative amplitude of the perturbations, which we consider to be constant over the flame length, $\omega = 2\pi f$ represents the angular frequency related to the modulation and $\kappa(x) = \omega/u_0(x)$ is the local wavenumber. The wavenumber is here non-uniform as velocity disturbances' phase velocity may vary along the flame front. This propagation is qualitatively depicted in Figure 6.

4.2. Local response of the flame

Small perturbations are assumed. We then start by expanding variables to first order:

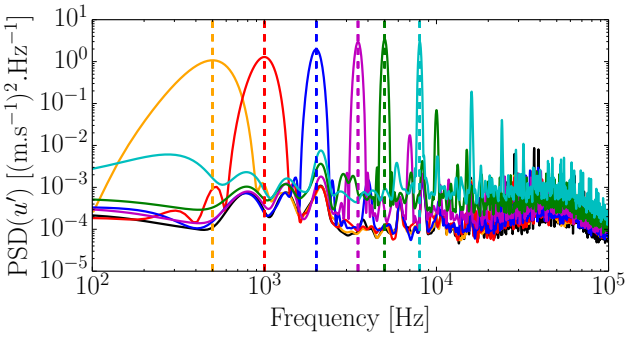

(a) Axial velocity component, annular jet, recorded 2 annulus thicknesses downstream of the injector

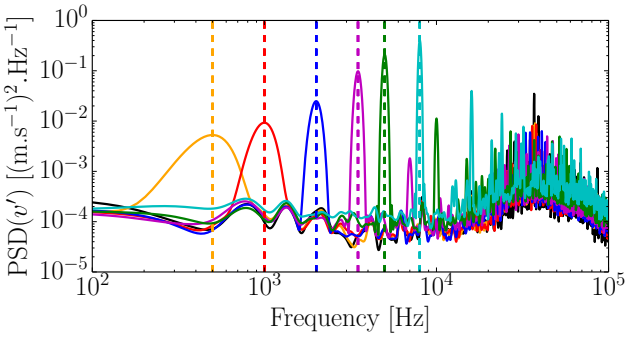

(b) Transverse velocity component, annular jet, recorded 2 annulus thicknesses downstream of the injector.

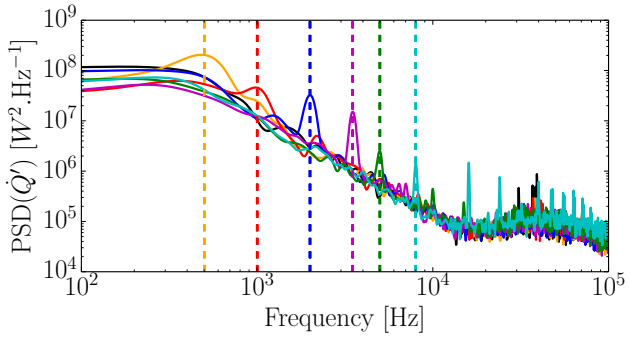

(c) Heat release rate integrated over the entire domain.

Figure 4: Power spectral densities of velocity and heat release rate signals computed using Welch's method, with 25 blocks, Hann's window, 50% overlapping, zero-padding. The spectral resolution is 203 Hz. Black: modulation-free case. Orange: $f = 500$ Hz. Red: $f = 1000$ Hz. Blue: $f = 2000$ Hz. Purple: $f = 3500$ Hz. Green: $f = 5000$ Hz. Cyan: $f = 8000$ Hz.

$$
\begin{aligned}
u(x,t) &= u_0(x) + u'(x,t), \\
\epsilon(x,t) &= \epsilon_0(x) + \epsilon'(x,t), \\
\dot{q}(x,t) &= \dot{q}_0(x) + \dot{q}'(x,t),
\end{aligned}
\tag{5}
$$

where the subscript 0 denotes a temporal average and $'$ a perturbation around the average. Here $\dot{q}$ is the surface heat release rate and ϵ the flame stretch rate. Considering our one-dimensional flame, with x the axial coordinate, the modulated rate of stretch within the annular jet $\tilde{\epsilon}'(x,t)$ imposed by the velocity modulation is given by:

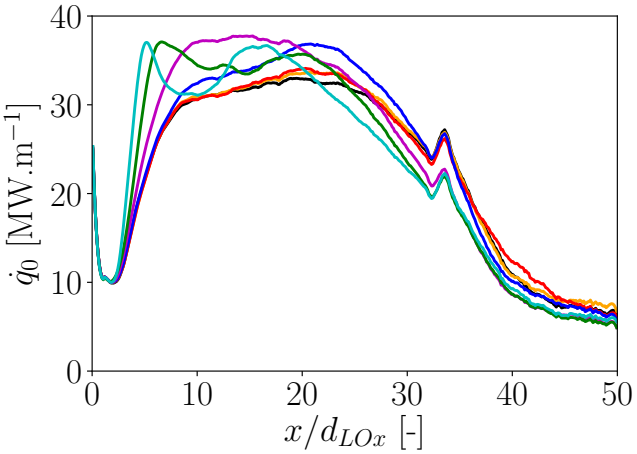

Figure 5: Distribution of the time averaged heat release rate over the flame axis after integration over the transverse directions (y and z) of the domain. Black: modulation-free case. Orange: $f = 500$ Hz. Red: $f = 1000$ Hz. Blue: $f = 2000$ Hz. Purple: $f = 3500$ Hz. Green: $f = 5000$ Hz. Cyan: $f = 8000$ Hz.

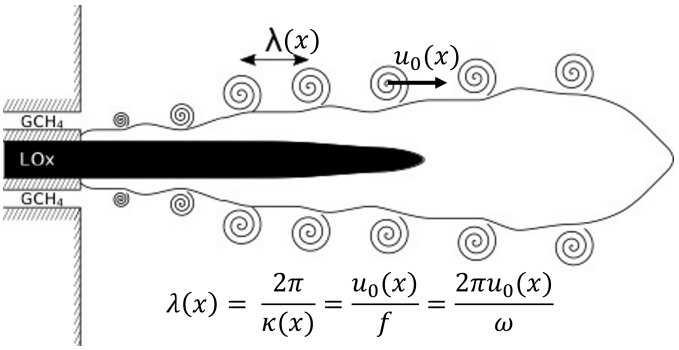

Figure 6: Schematic depicting the effect of the modulation on the flow with the transport of hydrodynamic disturbances at the annular jet mean velocity.

$$
\tilde{\epsilon}'(x,t) = \nabla_t \cdot \mathbf{u}'_t(x,t) \approx \frac{\partial u'(x,t)}{\partial x}. \tag{6}
$$

The assumed harmonic velocity propagation along the flame then yields:

$$
\tilde{\epsilon}'(x,t) \approx -a u_0(x) \kappa(x) \cos(\omega t - \kappa(x) x). \tag{7}
$$

The change in surface heat release rate related to a flame stretch rate disturbance can be thought of as the consequence of a contraction or expansion of species concentrations and temperature fields and hence of the resulting modification of diffusive fluxes. There is however a time delay characterizing this conversion of hydrodynamic

stretching into enhanced scalar diffusion across the shear layer, which results from the conservation equations governing the flow. The instantaneous heat release rate response of an unsteady flame then depends on the entire time history of the rate of stretch imposed by the flow. Haworth *et al.* [30] considered the problem of a counter-flow diffusion flame and solved it analytically. They demonstrated that, in the infinitely fast chemistry limit, a one-dimensional diffusion flame modulated by a flow exhibiting a fluctuating rate of stretch $\tilde{\epsilon}(x,t)$ burns with an effective flame stretch rate $\epsilon(x,t)$ - *i.e.* the stretch rate that would give the stationary flame with the same heat release rate - that verifies the following Bernoulli differential equation:

$$\frac{d\epsilon(x,t)}{dt} = -2\epsilon(x,t)^2 + 2\epsilon(x,t)\tilde{\epsilon}(x,t). \tag{8}$$

This temporal response of the effective flame stretch rate actually constitutes a second-order low-pass filter. By substituting for the actual flame stretch rate signal $\tilde{\epsilon}(x,t)$ from Eq. 7, linearizing the differential equation as small perturbations are assumed and integrating the equation, one can express the effective flame stretch rate disturbance field as shown by Candel [31]:

$$\begin{aligned}\epsilon'(x,t) = &- a\frac{u_0(x)\kappa(x)}{1+\left(\omega/\left(2\epsilon_0(x)\right)\right)^2} \\ &\times\left(\cos(\omega t-\kappa(x)x)+\frac{\omega}{2\epsilon_0(x)}\sin(\omega t-\kappa(x)x)\right),\end{aligned} \tag{9}$$

We now need to express the temporal response of heat release rate to a time varying flame stretch rate. Under a fast chemistry assumption and for a steady flame, heat release rate is a linear function of the square root of flame stretch rate (see for instance Pons *et al.* [26]):

$$\dot{q}(x) \propto \epsilon(x)^{1/2}. \tag{10}$$

Assuming small fluctuations $\epsilon'(x,t)$ around $\epsilon_0(x)$, one obtains:

$$\frac{\dot{q}'(x,t)}{\dot{q}_0(x)} = \frac{\epsilon'(x,t)}{2\epsilon_0(x)}. \tag{11}$$

By injecting Eq. 11 into Eq. 9, the space-time response of the flame in terms of surface heat release rate as a function of the modulated velocity signal takes the form:

$$\begin{aligned}\dot{q}'(x,t) = &- \frac{au_0(x)\kappa(x)}{2\epsilon_0(x)}\frac{\dot{q}_0(x)}{1+\left(\omega/\left(2\epsilon_0(x)\right)\right)^2} \\ &\times\left(\cos(\omega t-\kappa(x)x)+\frac{\omega}{2\epsilon_0(x)}\sin(\omega t-\kappa(x)x)\right).\end{aligned} \tag{12}$$

This equation can be integrated over the whole flame - *i.e.* to a distance where $\dot{q}_0(x)$ drops to zero - to determine the global heat release rate perturbation and deduce the corresponding relative level of fluctuation:

$$\begin{aligned}\frac{\dot{Q}'(t)}{\dot{Q}_0} = &- \frac{au_0(x)\kappa(x)}{2\epsilon_0(x)\dot{Q}_0}\int\frac{\dot{q}_0(x)}{1+\left(\omega/\left(2\epsilon_0(x)\right)\right)^2} \\ &\times\left(\cos(\omega t-\kappa(x)x)+\frac{\omega}{2\epsilon_0(x)}\sin(\omega t-\kappa(x)x)\right)dx,\end{aligned} \tag{13}$$

where $\dot{Q}'(t)$ is the total heat release rate fluctuation and $\dot{Q}_0$ the total average heat release rate. Strictly speaking, $\dot{Q}_0$ and $\dot{Q}'(t)$ are heat release rates per unit circumferential length. However, considering our simplified 1D model we can arbitrarily substitute surface quantities $\dot{q}$ with heat release rates per unit length in the x-direction, so that after integrating $\dot{Q}_0$ and $\dot{Q}'(t)$ actually represent total heat release rates. In this paper's illustrations and in the following theoretical developments, a lower-case q then denotes a heat release rate per unit length.

4.3. Assessment of the underlying assumptions

In order to validate the model constitutive relation between unsteady stretch rate and unsteady heat release rate and the subsequent linearization, local equations must be considered. From the Bernoulli equation Eq. 8 and assuming small disturbances around the mean and linearizing, the general response of the 'effective' flame stretch rate $\epsilon'(x,t)$ can be obtained from whatever input modulated rate of stretch $\tilde{\epsilon}'(x,t)$ signal (or velocity signal) by numerical integration of the linearized differential equation.
We recall that in previous sections a harmonic signal was considered yielding simple algebra. Here the outcome is a generalized version of Eq. 9 giving ϵ' as a function of space and time, which combined with Eq. 11, eventually yields the general, local and time-dependent surface heat release rate response to an arbitrary velocity solicitation of the annular jet:

$$\dot{q}'(x,t) = \dot{q}_0(x)e^{-2\epsilon_0(x)t}\int_0^t \epsilon'(x,\tau)e^{2\epsilon_0(x)\tau}d\tau. \tag{14}$$

In order to test this general equation locally all along the flame brush, flame stretch rates $\tilde{\epsilon}'(x,\tau)$ can be taken from the LES by extracting axial velocity signals, as well as $\dot{q}_0(x)$. The phase-locked solutions are employed in order to retain the modulation-induced coherent oscillations only. If we recall the origin of Eq. 8, the relevant velocity that yields the actual flame stretch rate when differentiated is the free stream velocity. In the case of the annular jet of a cryogenic flame, such a free stream velocity would be the plateau part of the top hat velocity profile that is found between the two mixing layers separating the annular jet from the oxygen jet and the surrounding gases

respectively. Indeed Eq. 8 represents momentum diffusion across the viscous mixing layer that separates the two jets. The domain being split in the direction of the flame axis into 2 mm thick slabs, the top hat maximum velocity in the annular jet is extracted by taking the maximum axial velocity found in each slab. LES flame stretch rates are deduced from these velocity signals by applying centered second-order finite differences to the signals. The flame stretch rate perturbation $\epsilon'(x,\tau)$ are then obtained. Additionally, the mean axial distribution of heat release rate $\dot{q}_0$ is extracted from the LES fields by integration of volumetric heat release rates over the slabs (see Figure 5). Employing such slabs permits to guarantee the extraction of sufficiently smooth datasets while retaining spatial resolution along the x-axis, which is consistent with the way we model the problem. It should however be noted that the choice was made not to use ϵ_0 resulting from the LES as we are still not sure what this filter cut-off driving parameter actually is in a non-laminar flow. A constant value of 100 s^{-1} was then used in what follows as it gave satisfactory results while being in a range within which the sensitivity of the output to this parameter is not so strong. After numerically integrating Eq. 14, the modulus and phase angle of the resulting flame heat release rate perturbation signal is computed. These are given on Figure 7 for several operating points, and confronted to the corresponding heat release rate disturbance signal extracted directly from the LES. The modulus is predicted within a maximum error margin of 30%. More importantly, the overall gain shape remains close to the direct heat release rate extraction from the LES. The phase angle is also efficiently recovered. In our sense this demonstrates that:

1. The flame stretch mechanism is the leading process inducing unsteady heat release rate in such modulated flames;
2. The differential equation Eq. 8 derived by Haworth [30] for a laminar stretched diffusion flame is a fair approximation of our yet complex turbulent problem;
3. The linear approximation holds for the amplitude considered in the present work (10% relative inlet velocity amplitude);
4. The one-dimensional reduction of the problem and the harmonic approximation made earlier for modeling the annular jet's free stream velocity signal are reasonable.

4.4. Model validation

Transfer functions between methane injection velocity and total heat release rate can be computed from both the LES and the model output signals:

$$F_{LES}(\omega) = \frac{\widehat{S}_{\dot{Q}'u'}(\omega)}{\widehat{S}_{u'u'}(\omega)}, \tag{15}$$

where $\widehat{S}_{\dot{Q}'u'}$ is the cross-power spectrum of $\dot{Q}'$ and u' signals, and $\widehat{S}_{u'u'}$ is the power spectrum of u'. On Figure 8 are depicted the gain and phase predicted by the model into which we injected the mean annular velocity and mean heat release rate datasets taken from the non-modulated LES. It should be noted that switching to the mean field of any of the modulated LES has very little effect on the resulting gain and phase. The curves shown in Figure 8, resulting from the non-modulated case, tend to indicate that a single non-modulated simulation of an injector element, together with such a reduced-order model, offer some interesting flame response prediction opportunities. The gain is indeed evaluated very accurately for all frequencies, while the phase behavior as predicted by the model still shows some limitations when confronted to direct LES results.

5. Summary and conclusions

The dynamics of a fuel-modulated transcritical coaxial flame is considered in this article. Large-Eddy Simulations show the production and convection of vortical structures along the flame front, the flame opening angle remaining low and the flow mainly axial. A low-order model representing the unsteady heat release rate produced by a fluctuating annular fuel injection velocity is derived for small disturbances. It assumes that the modulation of the injection rate produces hydrodynamic disturbances that act on the flame front by inducing fluctuating flame stretch rates. Using a one-dimensional approach, the perturbed velocity field is modeled by a traveling harmonic signal. Assuming that chemical times are short compared to mixing times, the temporal response of the total heat release rate of the flame can be expressed. The coupling between fluctuating stretch rate in the annular jet and heat release rate which constitutes the basis of our modeling approach is confirmed by locally confronting our theoretical predictions to LES data. It is eventually shown that one can access accurate gain predictions by feeding the model with the time-averaged results of a single non-modulated simulation of the flame while phase estimates show somewhat larger errors.

6. Acknowledgments

This work is part of an ongoing PhD thesis which is cofunded by CNES, the French national space agency and ArianeGroup, the prime contractor for the European launcher Ariane 5. It was also carried out in the framework of the French-German initiative REST (Rocket Engine STability). We are thankful to CERFACS for sharing the solver AVBP with us and for contributing to the development of its real-gas extension. HPC resources of CINES (Centre Informatique National de l'Enseignement Supérieur) were made available by GENCI (Grand Equipement National de Calcul Intensif) through grant A0022-B06176.

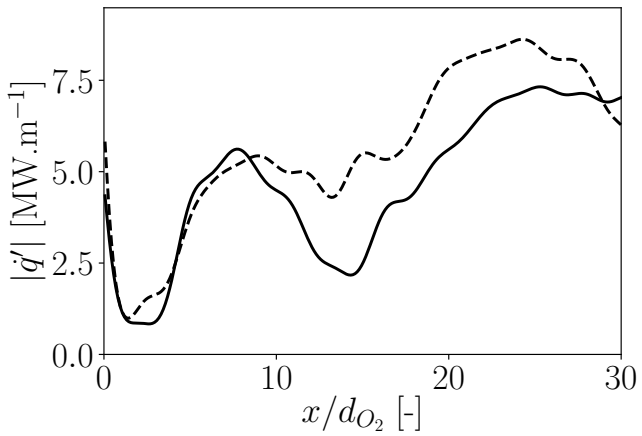

(a) Amplitude, 1000 Hz

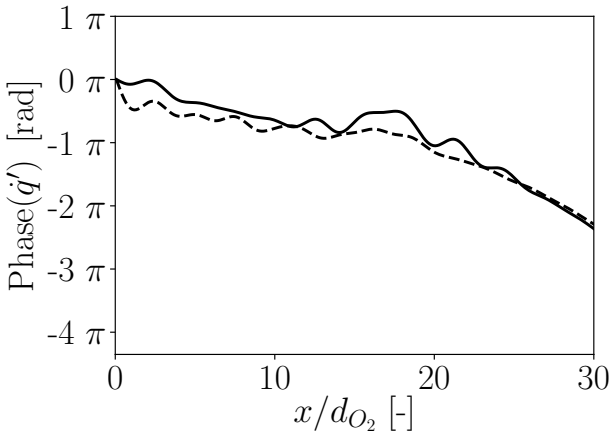

(b) Phase, 1000 Hz

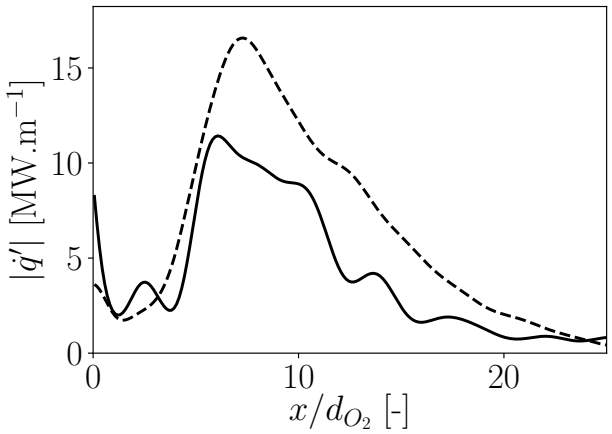

(c) Amplitude, 5000 Hz

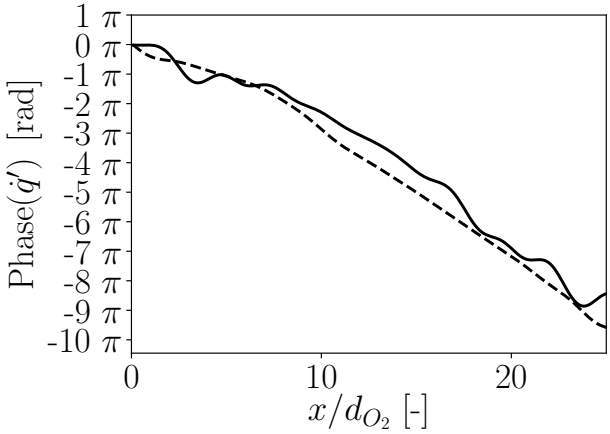

(d) Phase, 5000 Hz

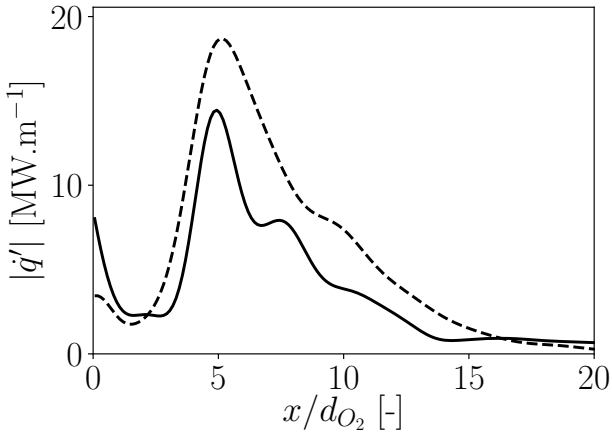

(e) Amplitude, 8000 Hz

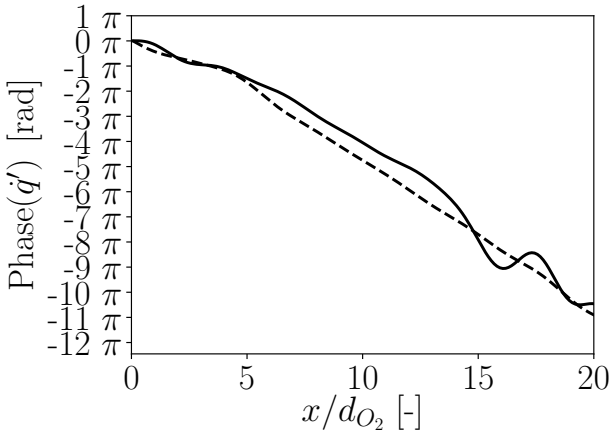

(f) Phase, 8000 Hz

Figure 7: Axial distribution of heat release rate amplitude and phase angle predicted by the model and confronted to LES outputs.

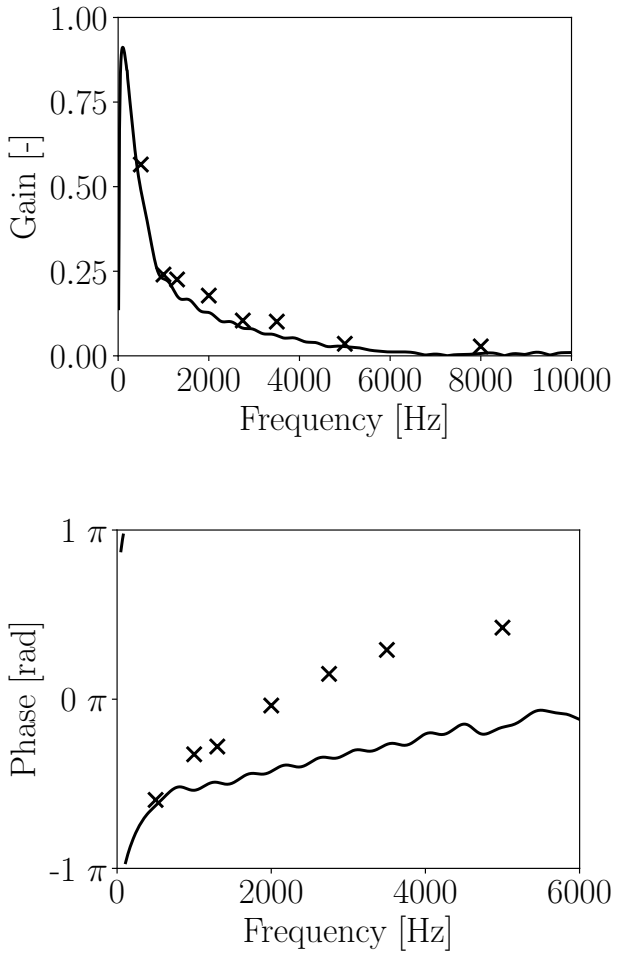

Figure 8: Gain and phase resulting from the LES (markers) and from the low-order model (continuous line). Bof the mean heat release rate axial distributions and the convective velocities are extracted from the LES.

[1] J. C. Oefelein, V. Yang, Comprehensive review of liquid-propellant combustion instabilities in f-1 engines, Journal of Propulsion and Power 9 (1993) 657–677.

[2] F. E. C. Culick, Unsteady motions in combustion chambers for propulsion systems. AGARDograph, Technical Report, NATO/RTO-AG-AVT-039, 2006.

[3] W. Anderson, V. Yang, Liquid rocket engine combustion instability, Progress in Astronautics and Aeronautics 169 (1995).

[4] L. Hakim, A. Ruiz, T. Schmitt, M. Boileau, G. Staffelbach, S. Ducruix, B. Cuenot, S. Candel, Large eddy simulations of multiple transcritical coaxial flames submitted to a high-frequency transverse acoustic modulation, Proceedings of the Combustion Institute 35 (2015) 1461–1468.

[5] A. Urbano, L. Selle, G. Staffelbach, B. Cuenot, T. Schmitt, S. Ducruix, S. Candel, Exploration of combustion instability triggering using large eddy simulation of a multiple injector liquid rocket engine, Combustion and Flame 169 (2016) 129–140.

[6] S. Candel, C. Huynh, T. Poinsot, Some modeling methods of combustion instabilities, in: Unsteady combustion, Springer, 1996, pp. 83–112.

[7] J. Pieringer, T. Sattelmayer, F. Fassl, Simulation of combustion instabilities in liquid rocket engines with acoustic perturbation equations, Journal of propulsion and power 25 (2009) 1020–1031.

[8] L. Hakim, Y. Méry, P. Scouflaire, S. Ducruix, S. Candel, Transcritical combustion dynamics analysis: high fidelity large eddy simulations vs reduced order modeling, in: French/German/United States Joint Symposium on Liquid Rocket Combustion Instabilities, London, UK, 2011.

[9] M. Schulze, T. Sattelmayer, Eigenvalue analysis for the prediction of initial growth rates of thermoacoustic instability in rocket motors, in: 53rd AIAA Aerospace Sciences Meeting, 2015, p. 1606.

[10] N. Noiray, D. Durox, T. Schuller, S. Candel, Mode conversion in acoustically modulated confined jets, AIAA journal 47 (2009) 2053–2062.

[11] L. Hakim, T. Schmitt, S. Ducruix, S. Candel, Dynamics of a transcritical coaxial flame under a high-frequency transverse acoustic forcing: Influence of the modulation frequency on the flame response, Combustion and Flame 162 (2015) 3482–3502.

[12] G. Singla, P. Scouflaire, J. C. Rolon, S. Candel, Transcritical oxygen/transcritical or supercritical methane combustion, Proceedings of the combustion institute 30 (2005) 2921–2928.

[13] M. Juniper, A. Tripathi, P. Scouflaire, J. C. Rolon, S. Candel, Structure of cryogenic flames at elevated pressures, Proceedings of the Combustion Institute 28 (2000) 1103–1109.

[14] T. Schonfeld, M. Rudgyard, Steady and unsteady flow simulations using the hybrid flow solver avbp, AIAA journal 37 (1999) 1378–1385.

[15] N. Gourdain, L. Gicquel, M. Montagnac, O. Vermorel, M. Gazaix, G. Staffelbach, M. Garcia, J. F. Boussuge, T. Poinsot, High performance parallel computing of flows in complex geometries: I. methods, Computational Science & Discovery 2 (2009) 015003.

[16] O. Colin, M. Rudgyard, Development of high-order taylor–galerkin schemes for les, Journal of Computational Physics 162 (2000) 338–371.

[17] K. W. Thompson, Time dependent boundary conditions for hyperbolic systems, Journal of computational physics 68 (1987) 1–24.

[18] T. J. Poinsot, S. K. Lele, Boundary conditions for direct simulations of compressible viscous flows, Journal of computational physics 101 (1992) 104–129.

[19] L. Selle, F. Nicoud, T. Poinsot, Actual impedance of nonreflecting boundary conditions: Implications for computation of resonators, AIAA journal 42 (2004) 958–964.

[20] L. Pons, N. Darabiha, S. Candel, T. Schmitt, B. Cuenot, The structure of multidimensional strained flames under transcritical conditions, Comptes Rendus Mecanique 337 (2009) 517–527.

[21] T. Schmitt, L. Selle, B. Ruiz, A .and Cuenot, Large-eddy simulation of supercritical-pressure round jets, AIAA journal 48 (2010) 2133–2144.

[22] T. Schmitt, Y. Méry, M. Boileau, S. Candel, Large-eddy simulation of oxygen/methane flames under transcritical conditions, Proceedings of the Combustion Institute 33 (2011) 1383–1390.

[23] G. Soave, Equilibrium constants from a modified redlich-kwong equation of state, Chemical Engineering Science 27 (1972) 1197–1203.

[24] T. H. Chung, M. Ajlan, L. L. Lee, K. E. Starling, Generalized multiparameter correlation for nonpolar and polar fluid transport properties, Industrial & engineering chemistry research 27 (1988) 671–679.

[25] F. Nicoud, F. Ducros, Subgrid-scale stress modelling based on the square of the velocity gradient tensor, Flow, Turbulence and Combustion 62 (1999) 183–200.

[26] L. Pons, N. Darabiha, S. Candel, Pressure effects on non-premixed strained flames, Combustion and Flame 152 (2008) 218–229.

[27] R. H. Kraichnan, Diffusion by a random velocity field, Physics of Fluids (1958-1988) 13 (1970) 22–31.

[28] T. Passot, A. Pouquet, Numerical simulation of compressible homogeneous flows in the turbulent regime, Journal of Fluid Mechanics 181 (1987) 441–466.

[29] T. Poinsot, D. Veynante, Theoretical and numerical combustion, RT Edwards, Inc., 2005.

[30] D. C. Haworth, M. C. Drake, S. B. Pope, R. J. Blint, The importance of time-dependent flame structures in stretched laminar flamelet models for turbulent jet diffusion flames, in: Symposium (International) on Combustion, volume 22, Elsevier, 1989, pp. 589–597.

[31] S. Candel, Combustion dynamics and control: Progress and challenges, Proceedings of the combustion institute 29 (2002) 1–28.